# In Vivo Imaging of the Photoreceptor Mosaic in Retinal Dystrophies and Correlations with Visual Function

*Stacey S. Choi,*[1] *Nathan Doble,*[2] *Joseph L. Hardy,*[3] *Steven M. Jones,*[4] *John L. Keltner,*[1,5] *Scot S. Olivier,*[4] *and John S. Werner*[1]

**Purpose.** To relate in vivo microscopic retinal changes to visual function in patients who have various forms of retinal dystrophy.

**Methods.** The UC Davis Adaptive Optics (AO) fundus camera was used to acquire in vivo retinal images at the cellular level. Visual function tests consisting of visual fields, multifocal electroretinography (mfERG), and contrast sensitivity were measured in all subjects by using stimuli that were coincident with areas imaged. Five patients with different forms of retinal dystrophy and three control subjects were recruited. Cone densities were quantified for all retinal images.

**Results.** In all images of diseased retinas, there were extensive areas of dark space between groups of photoreceptors, where no cone photoreceptors were evident. These irregular features were not seen in healthy retinas, but were apparent in patients with retinal dystrophy. There were significant correlations between functional vision losses and the extent to which these irregularities, quantified by cone density, occurred in retinal images.

**Conclusions.** AO fundus imaging is a reliable technique for assessing and quantifying the changes in the photoreceptor layer as disease progresses. Furthermore, this technique can be useful in cases where visual function tests provide borderline or ambiguous results, as it allows visualization of individual photoreceptors. (*Invest Ophthalmol Vis Sci.* 2006;47: 2080–2092) DOI:10.1167/iovs.05-0997

Retinal dystrophies are debilitating and currently incurable diseases that cause severe visual impairment from a young age. Patients with cone and cone–rod dystrophies typically exhibit visual acuity loss, visual field impairment, color vision deficiency, photophobia, and sometimes, nystagmus,[1–7] whereas patients with retinitis pigmentosa (RP), rod, or rod–cone dystrophies show night blindness, peripheral visual field depressions, or scotomas and, in some patients, residual central vision.[8]

Electroretinography (ERG) has been the most important objective tool in monitoring the progression of retinal dystrophies. In assessing central retinal function, the multifocal electroretinogram (mfERG) has been used[9–12] and has demonstrated that small remaining responses in the macular region can be measured reliably in patients with RP.[12–14]

Color vision tests have also been used in monitoring the progression of retinal dystrophies, as the cones are affected in most cases. Fishman et al.[15] examined 67 patients with various types of RP for color vision defects using the Farnsworth-Munsell 100-hue test. They found that when an atrophic macular lesion was present or if visual acuity was less than 20/30, none of the patients had normal color vision. RP patients with cystoid macular edema tested better than patients with foveal lesions. Heckenlively et al.[16] evaluated color vision abnormalities in all forms of inherited cone–rod dystrophy. Thirty seven of 40 eyes had abnormal error scores on the Farnsworth-Munsell 100-hue test, even though the average visual acuity was 20/30. Tritanomalous defects were the most common finding in these patients. More recently, in a large psychophysical study, similar results were found: most of the patients with cone and cone–rod dystrophies exhibited marked color vision defects, and the magnitude of defects correlated with the loss of visual acuity.[17]

Foveal cone functions in patients with retinal dystrophy can be inferred from visual acuity and contrast sensitivity measurements.[18–25] In comparison to visual acuity, however, contrast sensitivity is a more sensitive indicator of abnormal central visual function in diseased retinas.[18–22] Patients with better visual acuity (20/30 or better; e.g., those with RP) showed substantially reduced contrast sensitivity, especially at high spatial frequencies, whereas patients with poor visual acuity (e.g., with cone dystrophy) showed normal sensitivity to lower spatial-frequency gratings.

Numerous histologic studies have demonstrated both rod and cone photoreceptor degeneration with progression of retinal dystrophies.[26–31] Photoreceptors are either missing or have shortened and severely distorted outer segments. A common biochemical defect has been identified in early-onset retinal dystrophies in three different species of animals: rats, mice, and dogs.[32–34] In each of these animals, there was evidence of an abnormality in cyclic nucleotide metabolism, leading to the death of photoreceptor cells. Mullen and Lavail[35] demonstrated that a failure of the phagocytic relationship between the photoreceptor cells and the RPE leads to degenerative changes in the photoreceptors in chimeric rats. Chaitin and Hall[36] showed more specifically that the defect is not in the initial part of the phagocytic mechanism (i.e., binding and recognition), but occurs in the middle stages of ingestion or engulfment in RCS rats.

Although a great deal of information has been learned through histologic studies, it can be limited by artifacts intro-

From the Departments of [1]Ophthalmology & Vision Science and [5]Neurology and Neurological Surgery, University of California Davis, Sacramento, California; [2]Iris AO, Inc., Berkeley, California; [3]Posit Science Corp., San Francisco, California; and the [4]Lawrence Livermore National Laboratory, Livermore, California.

Supported by National Eye Institute Grant EY014743, National Institute on Aging Grant AG04058, a Jules and Doris Stein RPB Professorship, and the Department of Energy Biomedical Engineering Program. Portions of this work were performed under the auspices of the U.S. Department of Energy by University of California Lawrence Livermore National Laboratory under contract No. W-7405-Eng-48.

Submitted for publication July 28, 2005; revised November 28, 2005; accepted March 14, 2006.

Disclosure: **S.S. Choi**, None; **N. Doble**, None; **J.L. Hardy**, None; **S.M. Jones**, None; **J.L. Keltner**, None; **S.S. Olivier**, None; **J.S. Werner**, None

The publication costs of this article were defrayed in part by page charge payment. This article must therefore be marked "*advertisement*" in accordance with 18 U.S.C. §1734 solely to indicate this fact.

Corresponding author: Stacey S. Choi, Department of Ophthalmology & Vision Science, University of California Davis, Sacramento, CA 95817; sschoi@ucdavis.edu.

**TABLE 1.** Summary of Clinical Findings for the 5 Subjects with Retinal Dystrophies

| **RCD 1** | **Female** | **Age: 33** | **Left Eye** | **VA: 20/25** | **Diagnosis: Rod–Cone Dystrophy** |
|---|---|---|---|---|---|
| History | Nyctalopia for 10 years. | | | | |
| Color Vision | D-15 panel: normal; anomaloscope: normal; Cambridge Color Test: normal. | | | | |
| Visual Field | HVF 24-2 SITA Std., size III test target, see Fig. 5a; foveal threshold: 37 dB; reliability: fixation loss, 0/16; false-positive errors, 2%; false-negative errors, 0%. | | | | |
| Fundus | RPE atrophy along the vessel arcade superiorly and inferiorly, with moderate number of bone spicules; RPE atrophy correlated with the HVF loss superiorly and inferiorly from the optic nerve; macula and optic nerve: normal. | | | | |
| ERG | Standard clinical ERG: abnormal photopically and scotopically | | | | |
| **RCD 2** | **Male** | **Age: 31** | **Left Eye** | **VA: 20/20** | **Diagnosis: Rod–Cone Dystrophy** |
| History | Nyctalopia for at least 4 years. | | | | |
| Color Vision | D-15 panel: normal; anomaloscope: normal; Cambridge Color Test: normal. | | | | |
| Visual Field | HVF 24-2 SITA Std., size III test target, see Fig. 5b; foveal threshold: 37 dB with MD of −12.49; reliability: fixation loss, 2/17; false-positive errors, 2%; false-negative errors, 4%. | | | | |
| Fundus | Peripheral pigmentary disturbance with 1 + cell in the vitreous cavity; ONH: 3–4/10 cup with no definite pallor; no definitive vessel attenuation. | | | | |
| ERG | Grossly abnormal photopically and scotopically (almost flat scotopic ERG); recordable waveform with photopic and flicker fusion, consistent with moderate advanced retinal degeneration. | | | | |
| **RCD 3** | **Male** | **Age: 33** | **Right Eye** | **VA: 20/20** | **Diagnosis: Rod–Cone Dystrophy** |
| History | Nyctalopia for at least 3 years. | | | | |
| Color Vision | D-15 panel: normal; anomaloscope: normal; Cambridge Color Test: normal. | | | | |
| Visual Field | HVF 24-2 SITA Std., size III test target, see Fig. 5c; foveal threshold: 38 dB with MD of −13.31; reliability: fixation loss, 1/17; false-positive errors, 1%; false-negative errors, 0%. | | | | |
| Fundus | RPE atrophy along the vessel arcade inferiorly, with mild bone spiculing; bone spicules also present nasally; some suggestion of mild pallor of the disc; some mild vessel narrowing more inferiorly than superiorly; RPE atrophy agrees well will with HVF loss with sparing of the central fovea and perimacular region. | | | | |
| ERG | Abnormal multifocal ERG consistent with a retinal degeneration. | | | | |
| **CRD** | **Male** | **Age: 44** | **Right Eye** | **VA: 20/80** | **Diagnosis: Cone–Rod Dystrophy** |
| History | Metamorphopsia and vision blurring for 10 years; nyctalopia for 10–15 years. | | | | |
| Color Vision | D-15 panel: abnormal; anomaloscope: abnormal; Cambridge Color Test: elevated threshold on all three cone axes. | | | | |
| Visual Field | HVF 10-2 FP., size III test target, see Fig. 5d. foveal threshold: 3 dB; reliability; fixation loss, 0/14; false-positive errors, 0%; false-negative errors, 0%. | | | | |
| Fundus | Circular patch of RPE atrophy in the central subfoveal region; moderate vascular attenuation throughout the retinal periphery; some mild temporal pallor of the disc. | | | | |
| ERG | Measured in 1996 and 2004; phototopic responses: reduced to 20% of normal; scotopic responses: abnormal but not nearly as reduced as photopic responses. | | | | |
| **JMD** | **Female** | **Age: 13** | **Left Eye** | **VA: 20/100** | **Diagnosis: Juvenile Macular Dystrophy** |
| History | Vision loss for several years; parents had been told of unusual macular appearance. | | | | |
| Color Vision | D-15 panel: abnormal; anomaloscope: abnormal; Cambridge Color Test: elevated threshold on all three cone axes | | | | |
| Visual Field | HVF 24-2 SITA Std; Size III test target, see Fig. 5e; foveal threshold: 22 dB; reliability: fixation loss, 1/20; false-positive errors, 0%; false-negative errors, 0%. | | | | |
| Fundus | RPE changes in the macula with a flat macular reflex; vessels and optic nerves are normal. | | | | |
| ERG | Photopic: normal; flicker fusion: normal; scotopic: slight prolongation of the b-wave. | | | | |

duced during preparation of the retina, which further complicates the interpretation of disease processes at different stages. With the availability of adaptive optics (AO), it is now possible to image individual photoreceptors in living human eyes.[37] Roorda reported the first AO images on a cone dystrophy patient and showed that the retina was patchy due to photoreceptor dropout.[38] An overview of high-resolution retinal imaging using AO is provided by Doble.[39] The ability to image photoreceptors in vivo and distinguish functional versus nonfunctional cells makes AO imaging a potentially powerful technique for diagnosing and monitoring the disease course of retinal dystrophies with greater accuracy and precision than has been previously possible. These images may also be useful to the basic scientist who is interested in understanding the relations between anatomic and physiological integrity of the cone mosaic and visual function.

For AO images to be useful tools for clinical and basic science applications involving retinal dystrophies, the relations between AO-image-derived measures of photoreceptor integrity and visual function must be understood. The purpose of this study was to quantify and correlate the changes observed in high-resolution AO retinal images with various visual function tests.

## METHODS

### Subjects

Five patients with different forms of retinal dystrophy of unknown family history and three control subjects were tested. The patients

**TABLE 2.** Characteristics of Control Subjects

| Subject | Gender | Age | Eye Tested | Visual Acuity |
|---|---|---|---|---|
| Control 1 | Male | 20 | Left | 20/15 |
| Control 2 | Male | 33 | Left | 20/15 |
| Control 3 | Female | 41 | Right | 20/15 |

included three with rod–cone dystrophy, one with cone–rod dystrophy, and one with juvenile macular dystrophy. The dystrophies were diagnosed in the patients based on clinical examinations including ERG and/or mfERG, visual field analysis, and fundus examination. The clinical findings of these patients are summarized in Table 1. All subjects with dystrophy had bilateral changes, therefore the eye with greater variation of visual field defects was chosen for the study. Table 2 summarizes the characteristics of three control subjects used in this study. All subjects ranged in age from 13 to 44 years, with either zero or minimal refractive error (i.e., less than −2 D for both spherical and astigmatic correction). Refractive error was corrected with trial lenses before AO retinal imaging and psychophysical testing. The autorefractor unit was used for the mfERG. The tenets of the Declaration of Helsinki were observed, and written informed consent was obtained after all procedures were fully explained and before any experimental measurements.

## Procedure

**Photoreceptor Imaging.** The pupil was dilated with 1 drop of 1% tropicamide followed by 1 drop of 2.5% phenylephrine. During testing, the subject's head and eye movements were minimized by using a bite bar with a dental impression and a fixation target made up of concentric circles with an arrow pointing at the location for fixation. All subjects reported being able to see the tip of the arrow.

Figure 1 shows the flood-illuminated AO fundus camera in operation at UC Davis. The system consists of two parts: (1) the AO control loop which measures and corrects the ocular aberrations (shown by the dark gray shading) and (2) the imaging camera and projector, which provide for imaging and vision testing, respectively (light gray).

*AO Control Loop.* Trial lenses were used to correct sphere and cylinder before the AO implementation. The subject was instructed to fixate on a target consisting of a series of concentric circles calibrated to different retinal eccentricities in degrees from the fovea. The fixation target subtended a visual angle of ±8°. A superluminescent laser diode (SLD; model L8414-04, Hamamatsu Photonics, Hamamatsu City, Japan) operating at 835 ± 20 nm was used to form a wavefront sensor (WFS) beacon on the retina. The corneal irradiance was 63.9 μW, incident through a 1-mm entrance pupil. This is a factor of 9 below the recommended ANSI Standard.[40] The SLD was coupled into the eye via a high-quality pellicle beamsplitter (National Photocolor, Rochester, NY) and was delivered slightly off the corneal pole, to avoid the corneal reflex.[41] The pellicle was optically flat in both transmission and reflection, which allowed for a reference laser to be coupled into the system from the opposite side for calibration and alignment purposes.

Upon reflection from the retina, the 7-mm diameter exit pupil was relayed to the deformable mirror (DM) via a 10× magnification telescope. The DM was manufactured by Litton ITEK (DM109, Lexington, MA) and has 109 actuators arranged in a hexagonal array below a continuous front-surface mirror. It has an approximate mirror stroke of ±2 μm. This conjugate pupil plane was then relayed to the WFS via reflection from a high-quality, hot mirror. The WFS was Shack-Hartmann based, comprising a lenslet array (24-mm focal length, 400-μm pitch; Adaptive Optics Associates, Inc., Cambridge, MA) and a charge-coupled device (CCD) camera (model CA-D7; Dalsa, Waterloo, Ontario, Canada) located in the back focal plane of the lenslet array. The 7-mm exit pupil was magnified onto the WFS by a factor of 1.14 and sampled by 20 lenslets across the pupil diameter. The DM was operated using direct slope control,[42] whereby individual DM actuators are pushed and the resultant Shack-Hartmann WFS spot deflections recorded. The resultant matrix was then inverted and used to calculate the required voltages to be sent to the actuators, directly from the

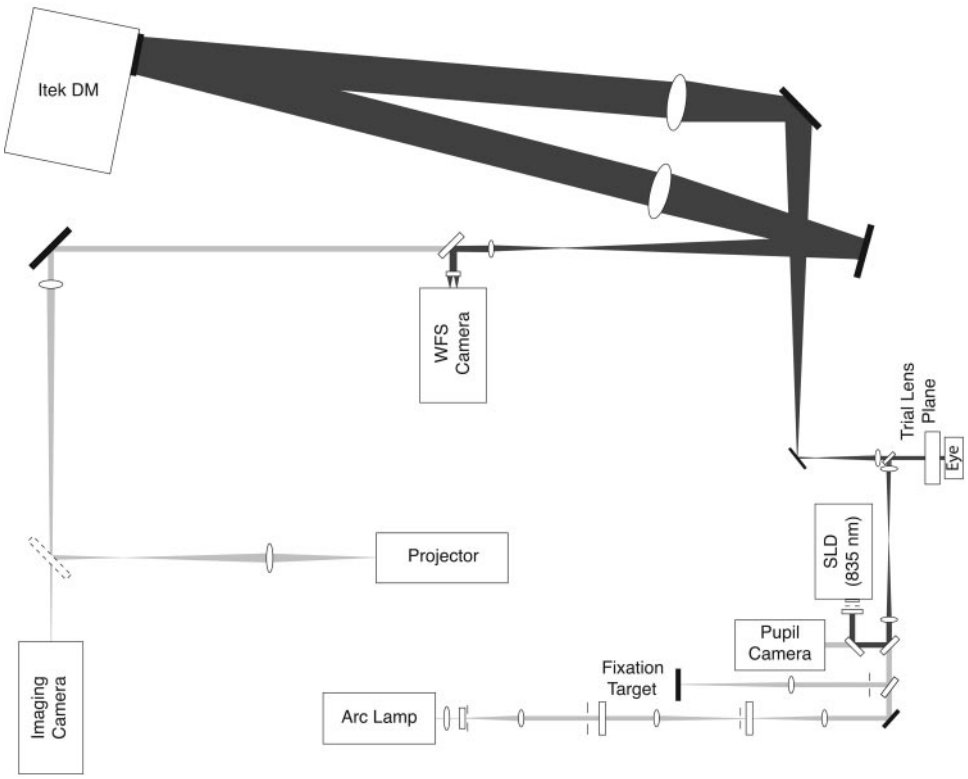


**FIGURE 1.** Flood-illuminated adaptive optics fundus camera at UC Davis. *Dark gray*: AO control loop; *light gray*: imaging and vision testing paths.

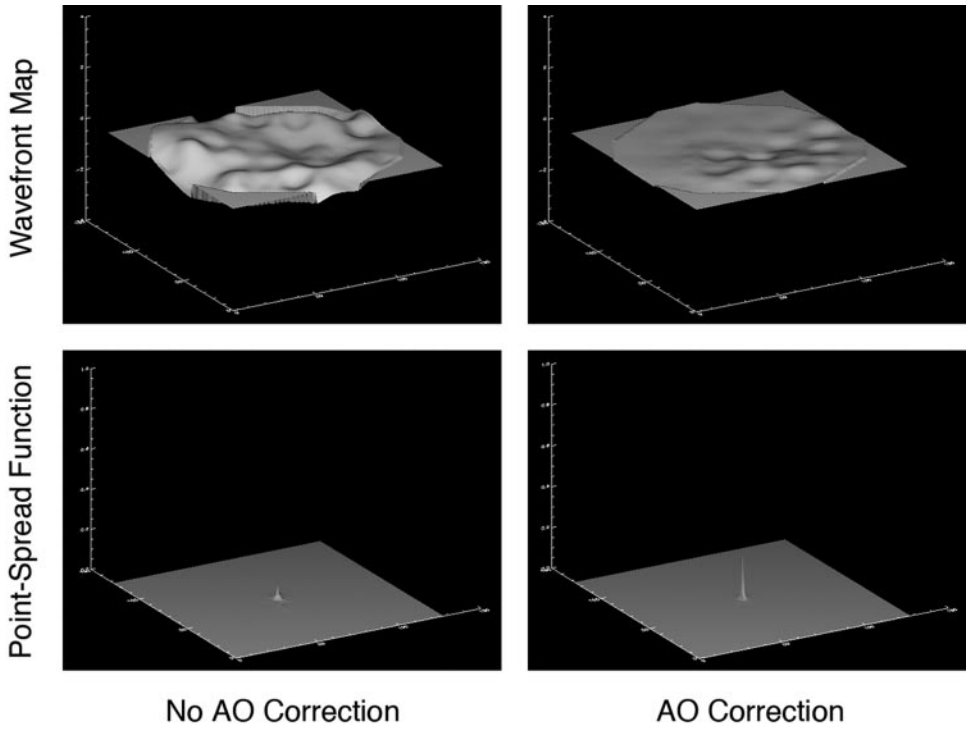


**FIGURE 2.** Wavefront (WF) and point-spread function (PSF) plots before and after AO correction over a 7-mm pupil. The WF became flatter after AO correction due to a decrease in RMS error by a factor of 3. The Strehl ratio of the PSF increased by a factor of 3.

measured slope offsets. This method removes the need for any wavefront reconstruction in the AO control loop. The aberrated wavefront was sampled at 20 Hz, providing an experimentally measured closed-loop bandwidth of ~0.9 Hz for a gain of 30%. Both the WFS and DM were controlled through a standard 2.66-GHz computer. Typical root mean square (RMS) correction for a 7-mm pupil was ~ 0.09 $\mu$m. Figure 2 shows the wavefront (WF) map before and after DM correction with the corresponding point-spread functions (PSFs). There was a decrease in RMS by a factor of 3 with an associated threefold increase in Strehl ratio. For imaging purposes, a smaller pupil of diameter 6.5 mm was used to avoid edge artifacts due to DM correction at the pupil margins.

*Imaging Camera.* Once the eye's aberrations were corrected, a shutter triggered retinal image acquisition. The imaging path is shown with the lighter gray shading in Figure 1. The imaging pulse followed the corrected path of the DM and was transmitted through the hot mirror to be re-imaged onto a cooled CCD camera (VersArray XP; Princeton Instruments, Monmouth, NJ). The imaging source was a 300-W xenon arc lamp regulated by a DC power supply (Oriel, Stratford, CT). The imaging wavelength is broadly tunable over the visible and near infrared spectrum by choice of an appropriate interference filter. The exposure duration was set to 10 ms with 0.6 and 0.25 $\mu$J of light being delivered through a 2.4-mm diameter entrance pupil using 40-nm full width at half maximum (FWHM) interference filters centered at 550 and 650 nm, respectively, a factor of 40 below the recommended International Commission on Non-Ionizing Radiation Protection (ICNIRP) guidelines.[43] The imaging camera was translated on a motorized axial stage to correct for the ocular longitudinal chromatic aberration between the WFS beacon at 835 nm and the visible wavelengths used for imaging.

The retinal image diameter was set to 1° with the size being controlled through an iris diaphragm located at a conjugate retinal plane in the flashlamp arm. To determine the system magnification, a model eye (consisting of a United States Airforce calibration target located in the front focal plane of a 50-mm focal length achromatic doublet lens) was placed in the eye pupil plane. The target was imaged onto the imaging camera and the magnification determined. For the given focal length doublet lens, the magnification agreed well with the theoretical prediction from optical design software (Zemax; Zemax Development Corp., San Diego, CA). Subsequently, in each subject, a measure of axial length and hence focal length allowed an accurate determination of the 1° retinal image in micrometers.

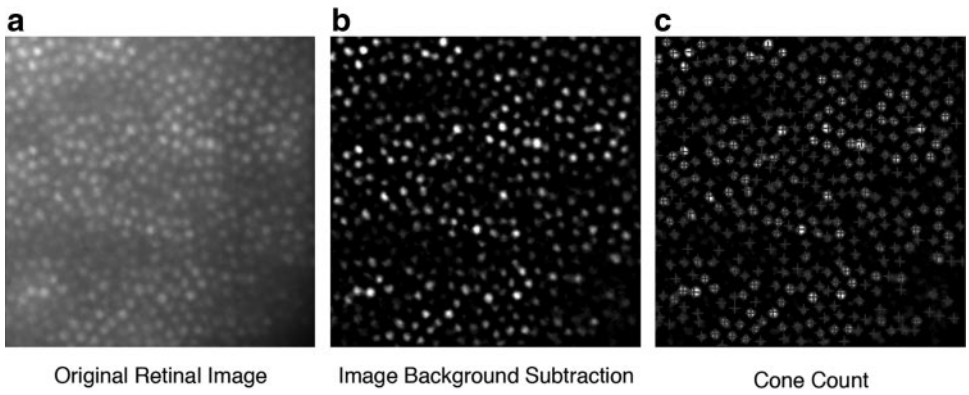


**FIGURE 3.** Illustration of the automated cone density measurement procedure. (**a**) Cropped original image; (**b**) image after background subtraction; (**c**) outcome of cone density measurement with all of the cones counted.

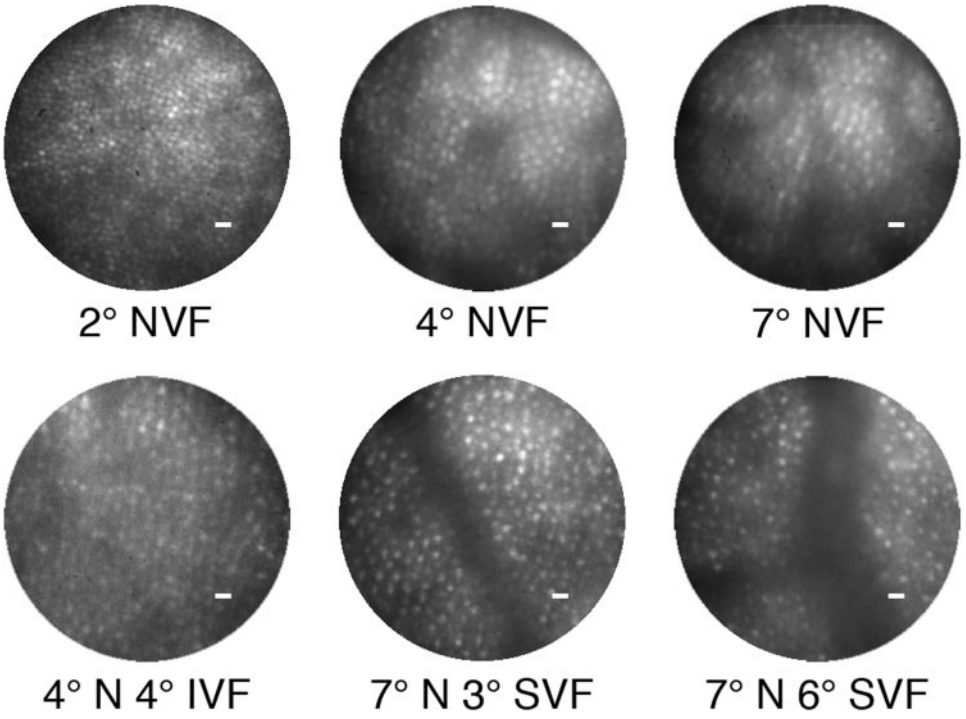


**FIGURE 4.** AO images of normal retina at six retinal locations from control subject 1. N, nasal; S, superior; I, inferior; VF, visual field. Scale bar, 10 $\mu$m.

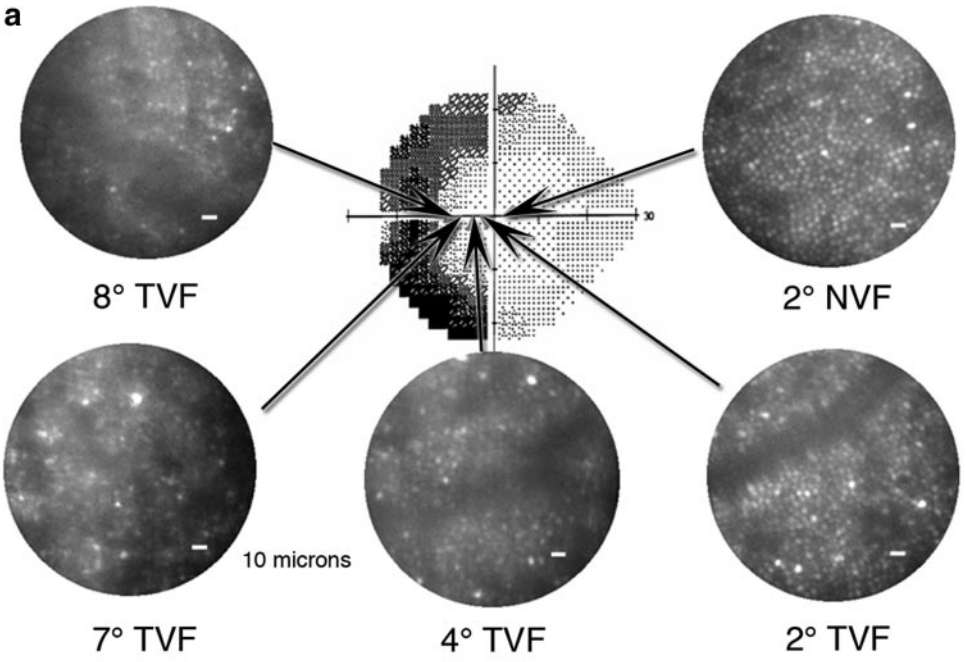


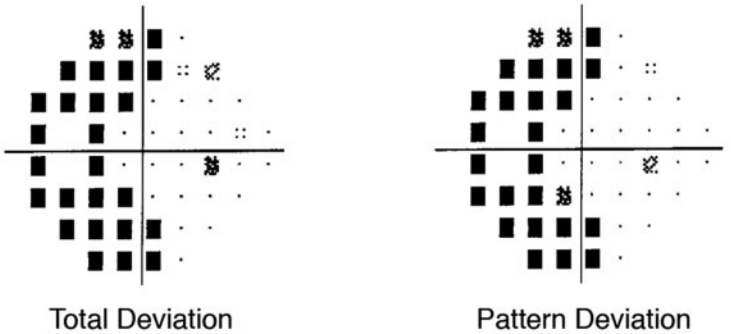


**FIGURE 5.** AO-corrected retinal images for each subject with a retinal dystrophy at different locations of the retina shown with the corresponding visual field maps. HVF 24-2 SITA Standard was used on all subjects except for the subject CRD, for whom HVF 10-2 FP was used. Retinal location is denoted in terms of visual field in degrees from the fovea. Data for the separate subjects are (**a**) RCD1, (**b**) RCD2, (**c**) RCD3, (**d**) CRD, and (**e**) JMD. Other details as in Figure 4.

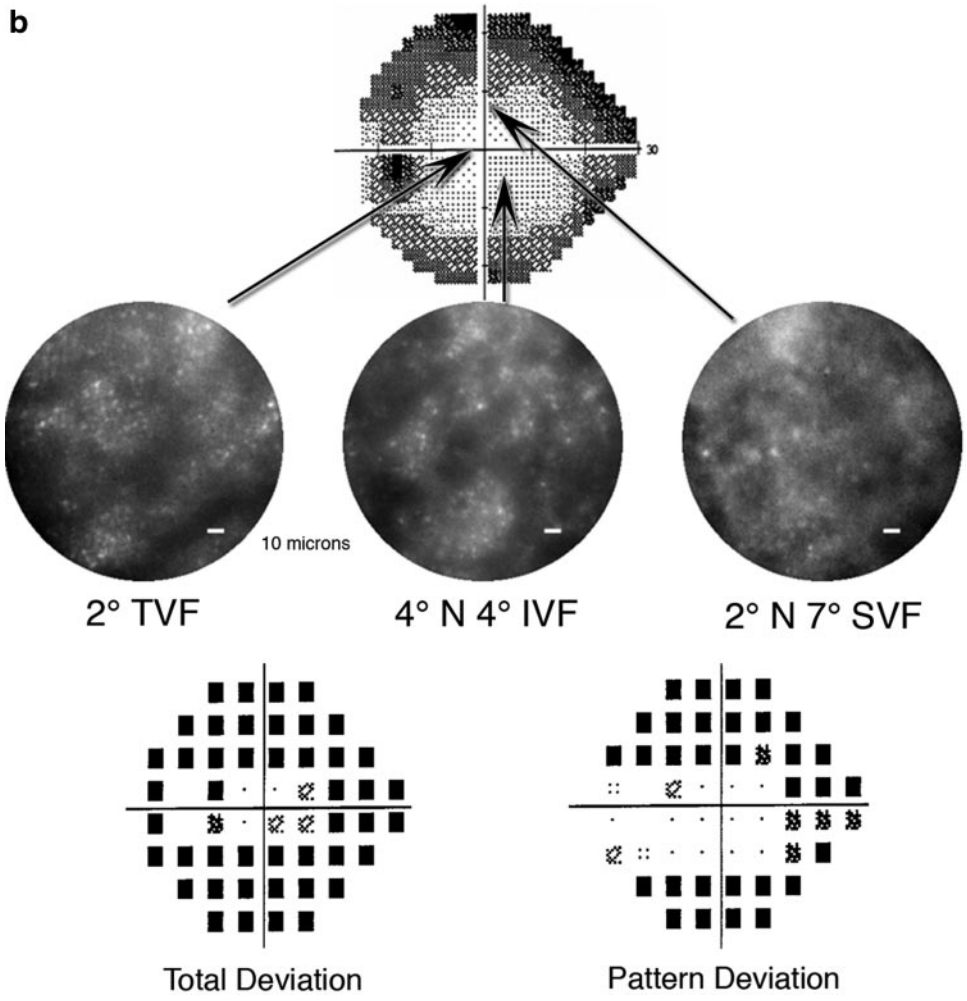


**FIGURE 5.** (*Continued*)

Approximately 30 to 40 images were taken at each retinal location for each subject. Of these, five to seven images were selected (based on image contrast and degree of overlap) and registered via an autocorrelation algorithm to optimize the contrast further and improve the signal-to-noise ratio.[44]

*Cone Density Measurement.* Photoreceptor density was determined by a computer routine (Matlab routine; The Mathworks, Inc., Natick, MA) that automatically counted the cones in the registered images. The initial, registered images, $I_{orig}$, were first convolved with a Gaussian filter and then subtracted from the initial profile to yield the new image intensity profile, $I$. The process is described by equation 1:

$$I = I_{orig} - I_{orig} \cdot e^{-(x^2+y^2)/2\sigma^2} \quad (1)$$

where the exponential describes a Gaussian filter of width $\sigma$ (the standard deviation) and $x$, $y$ denote the coordinates of a pixel.[45] For this work, a $\sigma$ of 30 was chosen. Figures 3a and 3b show the initial and filtered images, respectively. To aid visualization of the filtered images, the values of $I$ were linearly scaled to increase brightness.

By determining the intensity of the dimmest cone, a threshold intensity level could then be set. The intensity profile of the image was divided into smaller sections of 10 intensity levels to search for the pixels that were brighter than the threshold intensity in each section. Then, pairs of cones that were located closest to each other were selected in the image and their separations calculated from their $x$, $y$ coordinates in pixels. When a hot pixel fell within a locus defined by the smallest center-to-center cone spacing, the program ignored that pixel value. This step ensured that cones were counted only once. Figure 3c shows an example image with all the cones highlighted. It was then straightforward to calculate the cone density. This procedure was repeated five times, to work out the mean cone density. The variation between measurements was within 5% of the mean value.

**Functional Testing.** *Visual Field Analysis.* Prior to AO retinal imaging, visual fields were measured in each eye using a Humphrey Visual Field analyzer (HFA II–I series; Carl Zeiss Meditec, Inc., Dublin, CA) with SITA standard settings to determine the areas of reduced retinal sensitivity within the central 20 ° to 50° of visual field. Grayscale, total, and pattern deviation maps were used to pinpoint the locations of different retinal sensitivity. These maps were used to determine which eye and retinal locations to image using the AO fundus camera. All subjects had good fixation and response reliability during visual field testing. The fixation loss, false-positive and false-negative error scores are summarized for each subject in Table 1. A fixation target consisting of eight concentric rings spanning 1 ° to 8° in visual field was used to superimpose retinal imaging locations onto the locations of defects in the visual field maps. Depending on the severity of visual field loss, either a 24-2 or a 10-2 full threshold test was used with the size 3 stimulus (i.e., 3-mm circular stimulus on a white background [10 cd/m$^2$], with exposure duration of 200 ms).

*Multifocal Electroretinography.* The mfERG was used to isolate retinal response at discrete locations and to detect localized retinal dysfunction. The mfERG technique is based on a cross-correlation between hexago-

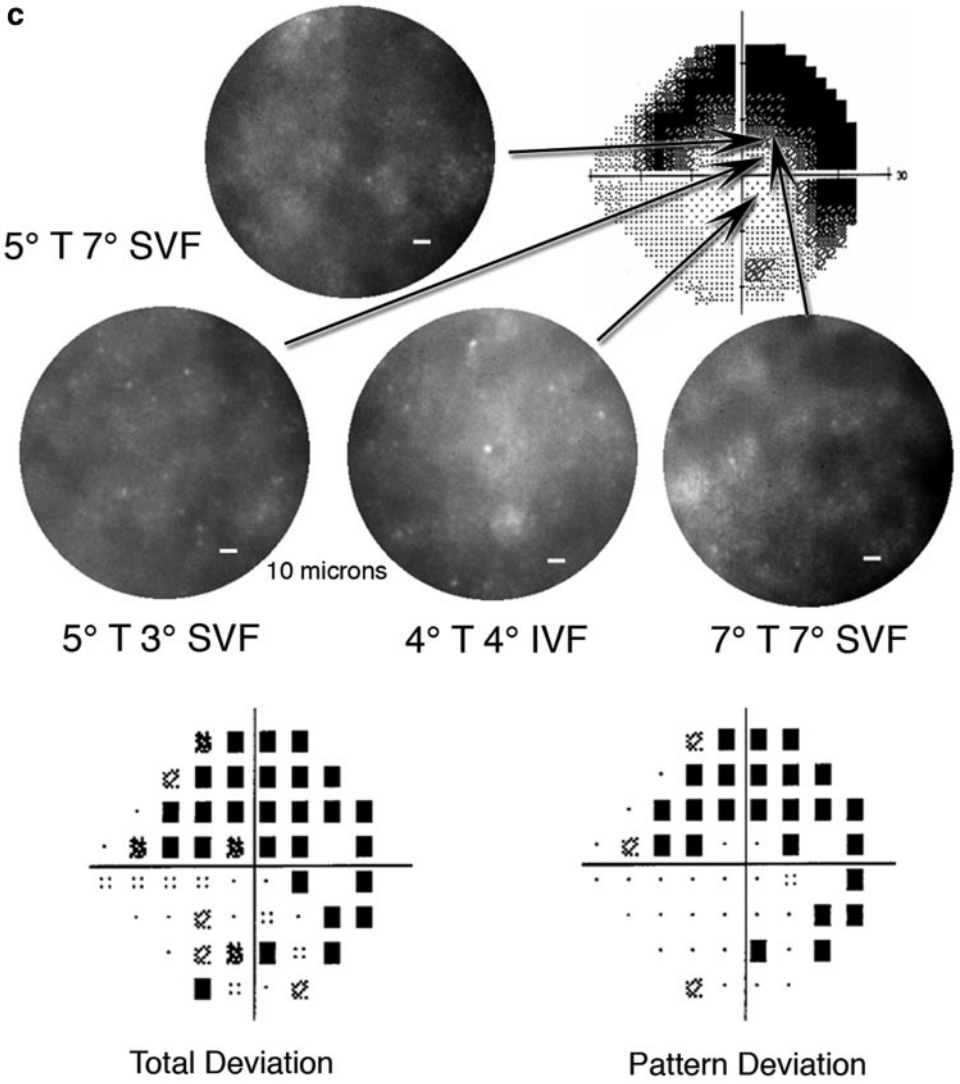


**FIGURE 5.** (*Continued*)

nal black-and-white stimulus changes and the local response of the retina, thus reflecting the first stage of retinal processing.[46] The protocol used was similar to the ISCEV (International Society for Clinical Electrophysiology of Vision) Guidelines for multifocal ERG and has been described in detail elsewhere.[47] Briefly, the recording was made under room light conditions with a dilated pupil (>6 mm; after instillation of 1 drop of 1% tropicamide and 1 drop of 2.5% phenylephrine). Correction of refractive error (between +6 and −6 D) was obtained using the refraction correction unit of the VERIS system (EDI, San Mateo, CA). The stimulus consisted of 103 hexagons that were not scaled with retinal eccentricity to facilitate comparison with the 1° retinal areas used for AO retinal imaging and contrast sensitivity testing. A central cross (+) was used for fixation. The flash intensity was 2.67 cd · sec/m$^2$ (200 cd/m$^2$), the intensity of the dark areas was less than 0.05 cd · sec/m$^2$ (<4 cd/m$^2$), and the frame rate was 75 Hz. Burian-Allen contact lens electrodes (Hansen Ophthalmic Development Laboratory, Iowa City, IA) were used as the active electrodes. Standard m-sequence stimulation mode (m = 14) required a recording time of 3.38 minutes. The responses were band-pass filtered between 10 and 300 Hz. Eight segments were used for each recording, and any segment contaminated by eye movements or artifacts was rejected and rerecorded. The pupil was continuously monitored with an infrared camera.

*Contrast Sensitivity.* The contrast sensitivity function (CSF) was measured with a 33-cm CRT video monitor (Multiscan G220; Sony, Tokyo, Japan) driven by a computer (Macintosh G4 with an ATI Radeon 7500 video card; 10-bits per gun). Gabor patches (sinusoidally modulated gratings windowed by a Gaussian envelope) were presented monocularly at the same size (1°) and corresponding retinal positions as the AO imaging. Contrast thresholds were measured at five spatial frequencies (1, 2, 4, 8, and 14 cyc/deg) using custom written software (written in Matlab 5.2.1; The MathWorks, with the Psychophysics Toolbox extension).[48,49] The monitor was characterized with a colorimeter (CS 100 Chroma Meter; Minolta) and gamma corrected by the procedures set forth in Brainard et al.[50] Subject position was stabilized by a forehead and chin rest, and the screen was viewed monocularly at a distance of 80 cm. All experiments were performed in a dark room. Before the CSF was measured, subjects were adapted for 10 minutes to the CRT screen by using the same space-average luminance as the test patches (31.3 cd/m$^2$). They were then asked to maintain steady central fixation by looking at a fixation target throughout the experiment. At each retinal location, the contrast sensitivity threshold for all five spatial frequencies, presented in random order, was measured with a QUEST adaptive tracking procedure.[51] The threshold value for each spatial frequency was taken as the geometric mean of the threshold estimated from two interleaved adaptive staircase tracks. The same procedure was repeated at the next retinal eccentricity. The subject's task was to judge in which of two temporal intervals the grating was presented and to record the response by pressing the corresponding button on the response pad.

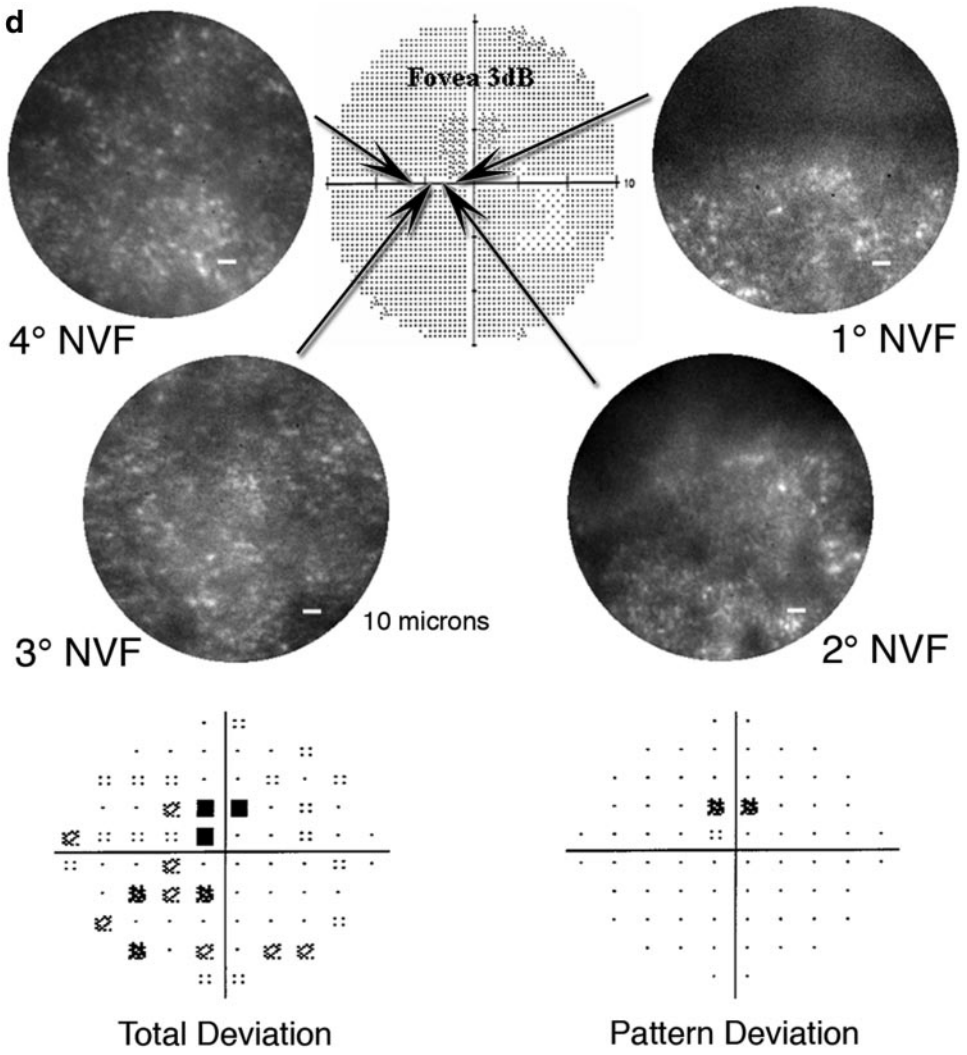


**FIGURE 5.** (*Continued*)

## RESULTS

Figure 4 shows the AO images of a normal retina (control subject 1) at six retinal locations. The scale bar represents 10 $\mu$m on the retina. The photoreceptor mosaic were regularly spaced in a hexagonal array across the retina. The cone diameter and the gaps between the cones increased with increasing eccentricity, as expected.[52]

Figures 5a, 5b, and 5c show the AO retinal images obtained from the three subjects with rod–cone dystrophy (RCD1, RCD2, and RCD3) at different retinal locations. The retinal locations tested were selected based on the visual field results so that areas with varying severity of functional loss could be imaged by the AO fundus camera. The consistent finding in all subjects with rod–cone dystrophy was that the cone mosaic is not regular (unlike that of normal eyes) at the retinal locations where sensitivity is reduced (i.e., there were areas of dark spaces between groups of cones, where no cones were visible). Figures 5d and 5e show the AO images from patients with cone–rod dystrophy (CRD) and juvenile macular dystrophy (JMD), respectively, at different retinal eccentricities. These subjects also showed photoreceptor irregularity at the locations where retinal sensitivity was reduced.

Cone density was calculated for each retinal image and is compared in Table 3 with the extrapolated cone densities from Curcio's histologic data at corresponding locations.[52] The relative percentage values provided an indication of relative cone loss at each retinal location. The variation in cone density from the least to the most affected areas was 96% to 49% for RCD1, 59% to 32% for RCD2, 33% to 22% for RCD3 (the three rod–cone dystrophy cases), 41% to 26% for CRD (cone–rod dystrophy), and 81% to 9% for JMD (juvenile macular dystrophy). These numbers provide a quantitative index of cone loss in various forms of retinal dystrophy.

The relation between cone density as measured by AO fundus photography and retinal sensitivity as measured by the Humphrey visual field (HVF) analyzer is shown in Figure 6. These data represent HFV sensitivity data for all regions in the five dystrophy subjects where AO fundus photography yielded cone density measurements. The HVF analyzer reports sensitivity data on a decibel scale. Visual inspection of the data relating these sensitivity measures and cone density clearly indicated that the *linear* sensitivity values would capture more of the variance in the cone density measurements in these dystrophic retinas. For the purposes of this analysis, HVF sensitivity is expressed as the linearized values

$$\text{Linear HVF sensitivity} = 10^{(\text{HVF sensitivity}/10)} \quad (2)$$

This operation simply inverts the decibel equation. When represented in this way, the linear relation between sensitivity and

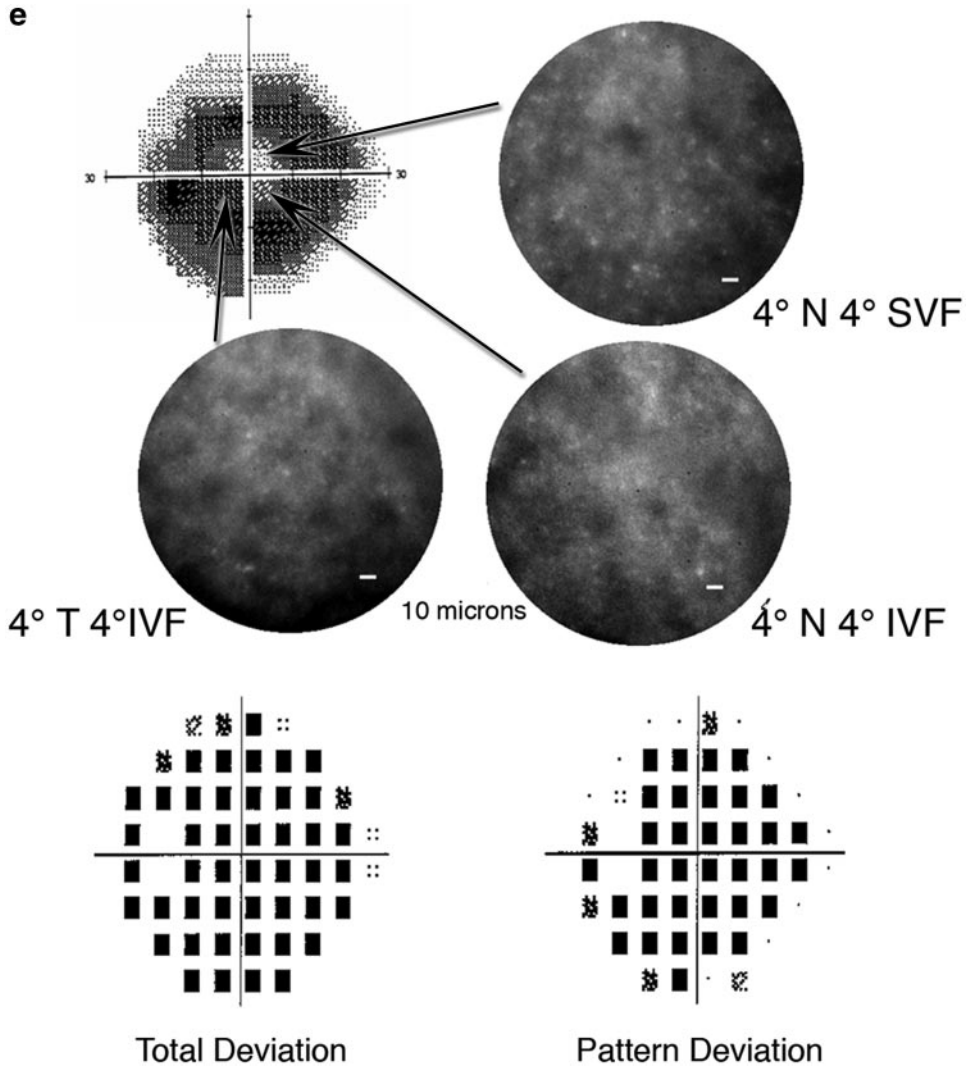


**FIGURE 5.** (*Continued*)

**TABLE 3.** Cone Density from AO Retinal Images for all Subjects

| Subject | Diagnosis | Retinal Location* | Cone Density Measurement (cells/mm$^2$) | Extrapolation from Curcio Data[52] (cells/mm$^2$) | Relative Cone Density from Histology (%) |
|---|---|---|---|---|---|
| RCD1 | Rod–cone dystrophy | 2° NVF | 41,450 | 43,000 | 96 |
| | | 2° TVF | 29,625 | 40,000 | 74 |
| | | 4° TVF | 15,075 | 25,000 | 61 |
| | | 7° TVF | 11,325 | 20,000 | 57 |
| | | 8° TVF | 7,825 | 16,000 | 49 |
| RCD2 | Rod–cone dystrophy | 2° TVF | 23,425 | 40,000 | 59 |
| | | 4° N 4° IVF | 10,525 | 20,000 | 53 |
| | | 2° N 7° SVF | 5,625 | 18,000 | 32 |
| RCD3 | Rod-cone dystrophy | 4° T 4° IVF | 6,500 | 20,000 | 33 |
| | | 5° T 3° SVF | 5,375 | 24,000 | 22 |
| | | 5° T 7° SVF | 4,550 | 18,000 | 25 |
| | | 7° T 7° SVF | 3,750 | 17,000 | 22 |
| CRD | Cone-rod dystrophy | 4° NVF | 20,300 | 25,000 | 81 |
| | | 3° NVF | 22,125 | 33,000 | 67 |
| | | 2° NVF | 13,200 | 43,000 | 31 |
| | | 1° NVF | 7,175 | 76,000 | 9 |
| JMD | Juvenile macular dystrophy | 4° N 4° SVF | 10,257 | 25,000 | 41 |
| | | 4° N 4° IVF | 7,075 | 20,000 | 35 |
| | | 4° T 4° IVF | 5,125 | 20,000 | 26 |

* The order in which retinal locations are listed is from the least to the most affected areas. N, nasal; T, temporal; S, superior; I, inferior; VF, visual field.

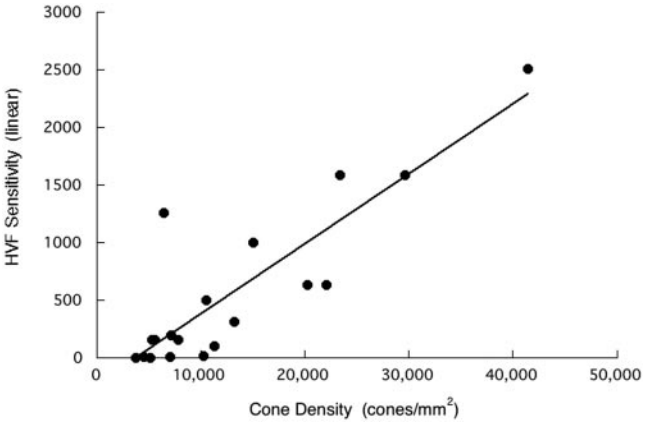


**FIGURE 6.** Linear HVF sensitivity (Equation 2) plotted as a function of cone density from all subjects with retinal dystrophy.

cone density becomes apparent. In fact, most of the variability in the HVF sensitivity measurements is explainable by the cone density measurements ($R^2 = 0.75$; $P < 0.01$).

The mfERG results are summarized in Figures 7a, 7b, and 7c for the rod–cone dystrophy subjects (RCD1, RCD2, and RCD3). The left figure in each panel shows the recordings from all 103 locations in the central 45° of the retina. The overall pattern of cone responses in the mfERG closely matched the visual field results, that is, the areas in the visual field that showed depression in retinal sensitivity were registered with flatter traces and longer latencies. The right figure shows the average cone responses from hexagons that correspond to the retinal locations used for AO imaging. The resolution of the mfERG is not fine enough to make a 1:1 correspondence with the AO imaging location. The size of each hexagon was calculated to be 4.4° on the retina. Therefore in some cases, a single hexagon represents the combined responses from more than one imaging location (e.g., in RCD1, trace 1 represents averaged response from the area that includes both 2° nasal visual field and 2° temporal visual field, whereas trace 3 includes 7° and 8° temporal visual fields). All three subjects with rod–cone dystrophy showed that as retinal sensitivity decreased, the mfERG trace became gradually flatter with longer latencies between peaks. Right images in Figures 7a, 7b, and 7c demonstrate this trend. The top trace represents averaged response from the retinal location that corresponds to healthier part(s) of the retina used for AO imaging. The bottom trace represents that of the most affected part of the retina imaged, and the middle trace(s) represent intermediate locations. At the retinal locations that were significantly affected by the disease, the amplitudes of mfERG evoked responses were reduced to near the noise level. Figures 7d and 7e show the mfERG recordings from subjects with cone–rod dystrophy (subject CRD) and juvenile macular dystrophy (subject JMD), respectively. Both subjects had no visible responses across all retinal locations tested (refer to second figure in Figs. 7d, and 7e). For subject CRD, trace 1 represents averaged response from the area that includes the 3° and 4° nasal visual fields, whereas trace 2 represents averaged responses that include the 1° and 2° nasal visual fields. To relate cone density to mfERG responses quantitatively, we chose the locations where responses above the noise level were obtained from the mfERG. When an mfERG response captured more than one of the cone regions imaged in AO, the cone densities from those areas were averaged. Figure 8 shows the relation between mfERG response density and cone density for the six regions where sufficiently adequate mfERG data were available from the subjects with dystrophy. Although this correlation is represented

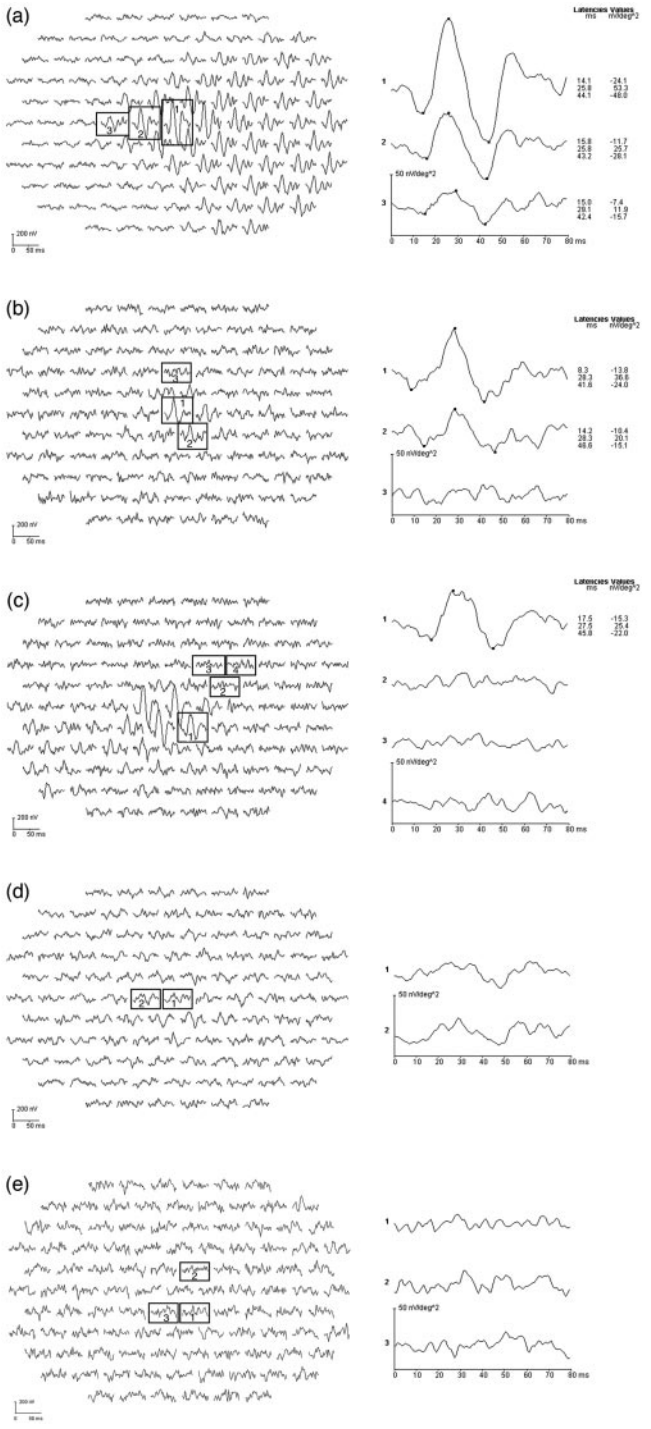


**FIGURE 7.** Multifocal ERG recordings showing the traces from all 103 hexagons as well as the ones that closely match the retinal locations used for AO imaging. (**a**) Subject RCD1; left eye with rod–cone dystrophy. The line plots (from *top to bottom*) correspond to average responses of 2° NVF and 2° TVF, 4° TVF and 7° TVF and 8° TVF, respectively. (**b**) Subject RCD2; left eye, with rod–cone dystrophy. The line plots correspond to 2° TVF, 4° N 4° IVF, and 2° N 7° SVF, respectively. (**c**) Subject RCD3; right eye, with rod–cone dystrophy. The line plots correspond to 4° T 4° IVF, 5° T 3° SVF, 5° T 7° SVF, and 7° T 7° SVF, respectively. (**d**) Subject CRD; right eye, with cone–rod dystrophy. The line plots correspond to average response of 3° and 4° NVF and of 1° and 2° NVF, respectively. (**e**) Subject JMD; left eye with juvenile macular dystrophy. The line plots (from *top to bottom*) correspond to 4° N 4° SVF, 4° N 4° IVF, and 4° T 4° IVF, respectively.

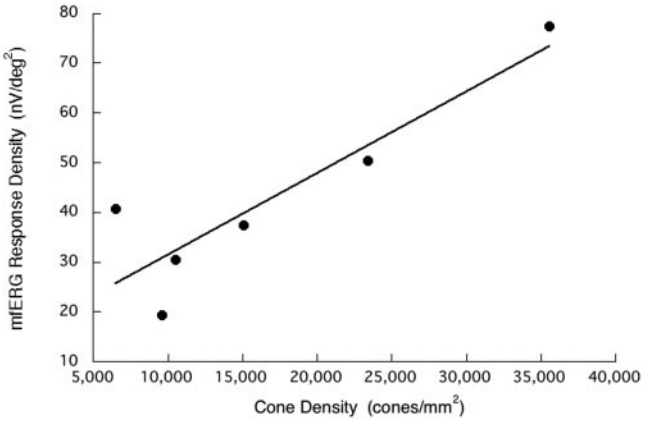


**FIGURE 8.** Response density of mfERG recordings plotted as a function of cone density from all subjects with retinal dystrophy. Measurable mfERG responses were obtained from six retinal locations across subjects.

by a small data set (six locations), the correlation is statistically significant ($R^2 = 0.80$, $P < 0.05$). There is a suggestion of a negative relation between cone density and response latency; however, the correlation with cone density fails to reach significance for both N1 and P1.

Figures 9a, 9b, and 9c show the luminance CSF from the three subjects with rod–cone dystrophy (RCD1, RCD2, and RCD3) at each retinal location, and corresponding CSFs from control subjects. Contrast sensitivity decreases were similar to the other functional tests and AO images, and disease-related reductions in contrast sensitivity were seen across all spatial frequencies tested. Figures 9d and 9e show the results from the subject with cone–rod dystrophy (CRD) and the one with juvenile macular dystrophy (JMD), respectively. The subject with cone–rod dystrophy had significantly reduced CSFs at all retinal locations compared with the control subject. These CSFs decreased in parallel with reduction in retinal sensitivity, as measured from other functional tests in the study. The subject with juvenile macular dystrophy did not have measurable contrast sensitivity at any of the retinal locations tested and therefore showed flat CSFs. To relate cone density to contrast sensitivity, we collapsed the CSF curves into a single value by averaging sensitivity across frequencies. Figure 10 shows the relation between mean contrast sensitivity and cone density for the retinal locations where AO images are available from the subjects with dystrophy. The linear relation was significant ($R^2 = 0.71$, $P < 0.01$). This relation is similar to that between linear HVF sensitivity and cone density, due to the strong correlation between mean contrast sensitivity and linear HVF sensitivity ($R^2 = 0.88$, $P < 0.01$).

## DISCUSSION

This study demonstrated a clear correlation between functional vision loss and the extent to which cone density decreases as measured from AO retinal images of retinal dystrophies. It is generally recognized that, regardless of differences in the underlying cause, the final common pathway of retinal degeneration is the apoptotic death of the photoreceptors.[26–31] Electron microscopic studies have revealed that cones of patients with retinal dystrophy have truncated outer segments that are composed of small groups of disoriented disc membranes and swollen inner segments. In the end, the course of the disease leads to the death of both inner and outer segments, leaving a residual photoreceptor cell of a spherical shape with little cytoplasm.[8] Such cell degeneration could explain the dark spaces seen in the AO retinal images. In healthy retinas, the photoreceptors reflect incident light from the junction of the inner and outer segments, and this light is wave-guided back through the pupil. Each bright spot in the AO image represents a dominant reflection from an individual photoreceptor.

When the cone density measurements from AO retinal images were compared with the mfERG recordings from corresponding areas, the analysis demonstrated a strong correlation

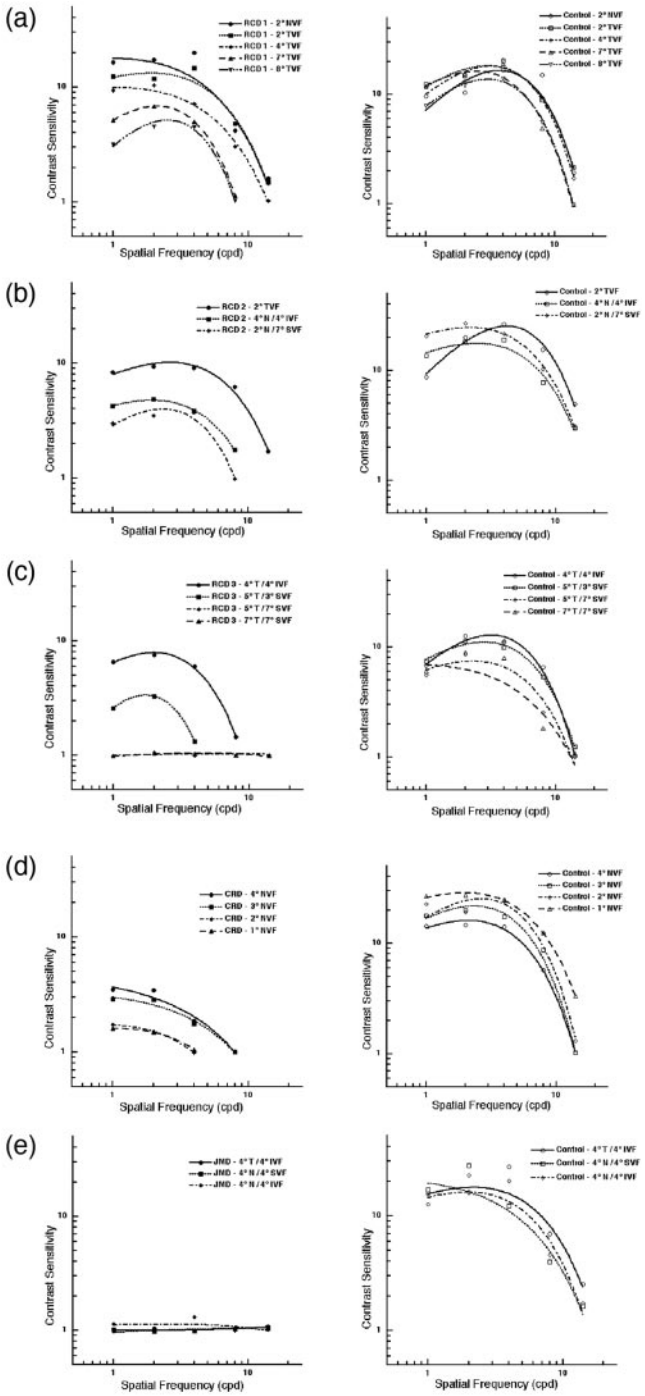


**FIGURE 9.** Contrast sensitivity functions for retinal dystrophy and control subjects at the retinal locations corresponding to those imaged with AO. Separate graphs denote the different subjects: (**a**) RCD1, (**b**) RCD2, (**c**) RCD3, (**d**) CRD, and (**e**) JMD.

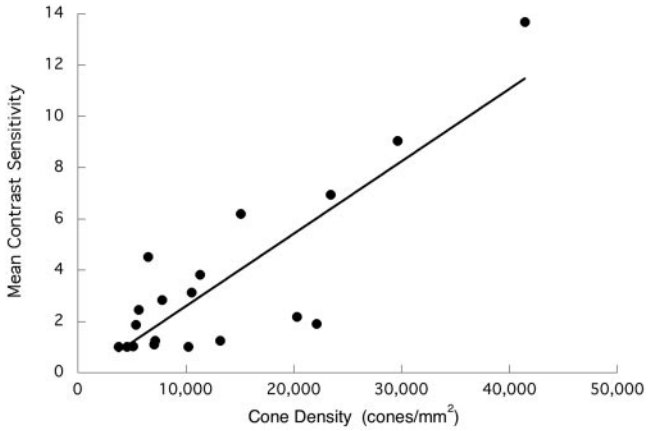


**FIGURE 10.** Mean contrast sensitivity is plotted as a function of cone density from all subjects with retinal dystrophy.

between response density and cone density ($R^2$ = 0.8; i.e., lower amplitudes of mfERG responses were associated with lower cone density measurements). While there is good agreement between AO fundus photography and mfERG in the assessment of the retinal dystrophy in this study, AO fundus photographs provided greater spatial localization and enabled the measurement of residual variation in relatively advanced disease.

Cone densities in patches of diseased retina are shown to be highly correlated with detection sensitivities for visual stimuli presented in those areas. The correlation between linear sensitivity measured with the HVF analyzer and cone photoreceptor density is strong ($R^2$ = 0.75) for the sample measured in this study. In addition, reductions in cone photoreceptor density are correlated with losses in contrast sensitivity ($R^2$ = 0.71). In contrast to previous findings, where contrast sensitivity was found to be mainly affected at higher spatial frequencies in diseased retinas,[18,22] contrast sensitivity decreased across all spatial frequencies in all of our subjects with retinal dystrophies. The CSFs for the juvenile macular dystrophy subject were flat at all retinal locations, indicating no residual functional vision at those locations.

This study confirms earlier histologic data[26–31] by showing apoptotic death of the photoreceptors in diseased retinas in vivo. The ability to monitor changes in the retinal mosaic of the living eye opens the possibility of (1) visualizing cellular changes without introducing artifacts from retinal preparation, (2) a more sensitive method of quantifying retinal changes, and (3) much earlier detection of any changes, which makes it possible to intervene with appropriate treatments at earlier stages of disease. This technology may also prove valuable in monitoring new therapeutic regimens.

This study thus demonstrates the applicability of the AO fundus camera in detecting cone losses as well as possibly monitoring the health of cone photoreceptors at a sensitivity level that cannot be attained with conventional clinical instruments. The objective measurements of cone photoreceptor integrity in this study (cone density) using AO imaging are highly correlated with measures of retinal function that are used both clinically and in research laboratories. These relations show the potential effectiveness of AO imaging for detecting and measuring the severity of retinal dystrophies. The ability to visualize the photoreceptor layer in vivo with AO imaging should be especially useful in cases in which visual function tests lead to ambiguous or borderline results, since the technique is potentially sensitive to the level of a single cone.

## *Acknowledgments*

The authors thank Susan Garcia and Adam White for assistance in testing; Bai Xue for assistance in software development; Christina Gerth for valuable comments; and Lawrence S. Morse, Susanna S. Park, and Edward Stone for assistance with diagnoses.

## *References*

1. Berson EL, Gouras P, Gunkel RD. Progressive cone-rod degeneration. *Arch Ophthalmol*. 1968;80:68–76.
2. Birch DG, Fish GE. Rod ERGs in retinitis pigmentosa and cone-rod degeneration. *Invest Ophthalmol Vis Sci*. 1987;28:140–150.
3. Fishman GA. Progressive human cone-rod dysfunction (dystrophy). *Trans Sect Ophthalmol Am Acad Ophthalmol Otolaryngol.* 1976;81:OP716–OP724.
4. Goodman G, Ripps H, Siegel IM. Cone dysfunction syndromes. *Arch Ophthalmol*. 1963;70:214–231.
5. Ripps H, Noble KG, Greenstein VC, Siegel IM, Carr RE. Progressive cone dystrophy. *Ophthalmology*. 1987;94:1401–1409.
6. Szlyk JP, Fishman GA, Alexander KR, Peachey NS, Derlacki DJ. Clinical subtypes of cone-rod dystrophy. *Arch Ophthalmol*. 1993;111:781–788.
7. Yagasaki K, Jacobson SG. Cone-rod dystrophy: phenotypic diversity by retinal function testing. *Arch Ophthalmol*. 1989;107:701–708.
8. Heckenlively JR. *Retinitis Pigmentosa.* Philadelphia, PA: JB Lippincott Company; 1988.
9. Sutter EE, Tran D. The field topography of ERG components in man. I. The photopic luminance response. *Vision Res*. 1992;32:433–446.
10. Bearse MA, Sutter EE. Imaging localized retinal dysfunction with the multifocal electroretinogram. *J Opt Soc Am A Opt Image Sci Vis*. 1996;13:634–640.
11. Gränse L, Abrahamsson M, Ponjavic V, Andréasson S. Electrophysiological findings in two young patients with Bothnia dystrophy and a mutation in the RLBP1 gene. *Ophthalmic Genet*. 2001;22:97–105.
12. Vajaranant TS, Seiple W, Szlyk JP, Fishman GA. Detection using the multifocal electroretinogram of mosaic retinal dysfunction in carriers of X-linked retinitis pigmentosa. *Ophthalmology*. 2002;109:560–568.
13. Gränse L, Ponjavic V, Andréasson S. Full field ERG, multifocal ERG and multifocal VEP in patients with retinitis pigmentosa and residual central visual fields. *Acta Ophthalmol Scand*. 2004;82:701–706.
14. Holopigian K, Seiple W, Greenstein VC, Hood DC, Carr RE. Local cone and rod system function in patients with retinitis pigmentosa. *Invest Ophthalmol Vis Sci*. 2001;42:779–788.
15. Fishman GA, Young RS, Vasquez V, Lourenco P. Color vision defects in retinitis pigmentosa. *Ann Ophthalmol*. 1981;13:609–618.
16. Heckenlively JR, Martin DA, Rosales TO. Telangiectasia and optic atrophy in cone-rod degenerations. *Arch Ophthalmol*. 1981;99:1983–1991.
17. Sadowski B, Zrenner E. Cone and rod function in cone degenerations. *Vision Res*. 1997;37:2303–2314.
18. Grover S, Fishman GA, Alexander KR, Anderson RJ, Derlacki DJ. Visual acuity impairment in patients with retinitis pigmentosa. *Ophthalmology*. 1996;103:1593–1600.
19. Marmor MF. Contrast sensitivity and retinal disease. *Ann Ophthalmol*. 1981;13:1069–1071.
20. Hyvärinen L, Rovamo J, Laurinen P, Peltomaa A. Contrast sensitivity function in evaluation of visual impairment due to retinitis pigmentosa. *Acta Ophthalmol*. 1981;59:763–773.
21. Wolkstein M, Atkin A, Bodis-Wollner I. Contrast sensitivity in retinal disease. *Ophthalmology*. 1980;87:1140–1149.
22. Sucs FE, Uvijls A. Contrast sensitivity in retinitis pigmentosa at different luminance levels. *Clin Vision Sci*. 1992;7:147–151.

23. Lindberg CR, Fishman GA, Anderson RJ, Vasquez V. Contrast sensitivity in retinitis pigmentosa. *Br J Ophthalmol*. 1981;65:855–858.
24. Akeo K, Hiida Y, Saga M, Inoue R, Oguchi Y. Correlation between contrast sensitivity and visual acuity in retinitis pigmentosa patients. *Ophthalmologica*. 2002;216:185–191.
25. Alexander KR, Derlacki DJ, Fishman GA. Contrast thresholds for letter identification in retinitis pigmentosa. *Invest Ophthalmol Vis Sci*. 1992;33:1846–1852.
26. Bunt-Milam A, Kalian R, Pagan R. Clinical-ultrastructural study of a retinal dystrophy. *Invest Ophthalmol Vis Sci*. 1983;24:458–469.
27. Flannery J, Farber D, Bird A, Book D. Degenerative changes in a retina affected with autonomic dominant retinitis pigmentosa. *Invest Ophthalmol Vis Sci*. 1989;30:191–211.
28. Szamier RB, Berson EL. Retinal ultrastructure in advanced retinitis pigmentosa. *Invest Ophthalmol Vis Sci*. 1977;16:947–962.
29. Szamier RB, Berson EL, Klein R, Meyers S. Sex-linked retinitis pigmentosa: ultrastructure of photoreceptors and pigment epithelium. *Invest Ophthalmol Vis Sci*. 1979;18:145–160.
30. Kolb H, Gouras P. Electron microscopic observations of human retinitis pigmentosa, dominantly inherited. *Invest Ophthalmol Vis Sci*. 1974;13:487–498.
31. Li Z, Jacobson S, Milam A. Autosomal dominant retinitis pigmentosa caused by the threonine-17 methionine rhodopsin mutation: retinal histopathology and immunocytochemistry. *Exp Eye Res*. 1994;58:397–408.
32. Lolley RN, Farber DB, Rayborn ME, Hollyfield JG. Cyclic GMP accumulation causes degeneration of photoreceptor cells: simulation of an inherited disease. *Science*. 1977;196:664–666.
33. Farber DB, Lolley RN. Enzymatic basis for cyclic GMP accumulation in degenerative photoreceptor cells of mouse retina. *J Cyclic Nucleotide Res*. 1976;2:139–148.
34. Aguirre G, Farber D, Lolley R, Fletcher RT, Chader GJ. Rod-cone dysplasia in Irish setters: a defect in cyclic GMP metabolism in visual cells. *Science*. 1978;201:1133–1134.
35. Mullen RJ, Lavail MM. Inherited retinal dystrophy: Primary defect in pigment epithelium determined with experimental rat chimeras. *Science*. 1976;192:799–801.
36. Chaitin MH, Hall MO. Defective ingestion of rod outer segments by cultured dystrophic rat pigment epithelial cells. *Invest Ophthalmol Vis Sci*. 1983;24:812–820.
37. Liang J, Williams DR, Miller DT. Supernormal vision and high resolution retinal imaging through adaptive optics. *J Opt Soc Am A*. 1997;14:2884–2892.
38. Roorda A. Adaptive optics ophthalmoscopy. *J Ref Surgery*. 2000; 16:S602–S607.
39. Doble N. High resolution, in vivo retinal imaging using adaptive optics and its future role in ophthalmology. *Expert Rev Med Devices*. 2005;2:205–216.
40. *American National Standard for the Safe Use of Lasers* ANSI Z136.1. New York: American National Standards Institute; 2000.
41. Hofer H, Artal P, Singer B, Aragón JL, Williams DR. Dynamics of the eye's wave aberration. *J Opt Soc Am A*. 2001;18:497–506.
42. Jiang W, Li H. Hartmann-Shack wavefront sensing and control algorithm. *Proc SPIE*. 1990;1271:82–93.
43. International Commission on Non-Ionizing Radiation Protection. Guidelines on limits of exposure to broad-band incoherent optical radiation (0.38–3 μm). *Health Physics.* 1997;73:539–554.
44. Brown LG. A survey of image registration techniques. *ACM Computing Surveys*. 1992;24:325–376.
45. Soliz P, Wilson M, Nemeth S, Nguyen P. Computer aided methods for quantitative assessment of longitudinal changes in retinal images presenting with maculopathy. *Proc SPIE*. 2002;4681:159–170.
46. Sutter EE. The fast m-transform: a fast computation of cross-correlations with binary m-sequences. *Soc Ind Appl Math*. 1991;20: 686–694.
47. Gerth C, Garcia SM, Ma L, Keltner JL, Werner JS. Multifocal electroretinogram: age-related changes for different luminance levels. *Graefes Arch Clin Exp Ophthalmol*. 2002;240: 202–208.
48. Brainard DH. The psychophysics toolbox. *Spat Vis*. 1997;10:433–436.
49. Pelli DG. The VideoToolbox software for visual psychophysics: transforming numbers into movies. *Spat Vis*. 1997;10:437–442.
50. Brainard DH, Pelli DG, Robson T. Display characterization. In: Hornak JP, ed. *Encyclopedia of Imaging Science and Technology.* New York: Wiley; 2002:72–188.
51. Watson AB, Pelli DG. QUEST: A Bayesian adaptive psychometric method. *Percept Psychophys*. 1983;33:113–120.
52. Curcio CA, Sloan KR, Kalina RE, Hendrickson AE. Human photoreceptor topography. *J Comp Neurol.* 1990;292:497–523.